Precise determination of force microscopy cantilever stiffness from dimensions and eigenfrequencies

Jannis Lübbe[1]**, Lutz Doering**[2] **and Michael Reichling**[1]

[1] Fachbereich Physik, Universität Osnabrück, Barbarastraße 7, 49076 Osnabrück, Germany
[2] Physikalisch-Technische Bundesanstalt (PTB), Nano- and Micrometrology, Bundesallee 100, 38116 Braunschweig, Germany

E-mail: reichling@uos.de and lutz.doering@ptb.de

Abstract

We demonstrate the non-destructive measurement of the stiffness of single-beam, monocrystalline silicon cantilevers with a trapezoidal cross-section and tips as used for atomic force microscopy from the knowledge of cantilever dimensions, eigenfrequencies and material parameters. This yields stiffness values with an uncertainty of $\pm 25\%$ as the result critically depends on the thickness of the cantilever that is experimentally difficult to determine. The uncertainty is reduced to $\pm 7\%$ when the measured fundamental eigenfrequency is included in the calculation and a tip mass correction is applied. The tip mass correction can be determined from the eigenfrequencies of the fundamental and first harmonic modes. Results are verified by tip destructive measurements of the stiffness with a precision instrument recording a force–bending curve yielding an uncertainty better than $\pm 5\%$.

S Online supplementary data available from stacks.iop.org/MST/23/045401/mmedia

(Some figures may appear in colour only in the online journal)

1. Introduction

The stiffness of the cantilever used in atomic force microscopy (AFM) is an important property for quantitative imaging. The knowledge of the cantilever stiffness is, for instance, important for the precise determination of adhesion forces and free energy landscapes of biological objects investigated by contact-mode or intermittent contact AFM [1]. When operating the AFM in the non-contact mode (NC-AFM), the stiffness and eigenfrequency of the cantilever are, for instance, used to calculate the normalized frequency shift, greatly facilitating the quantitative comparison of NC-AFM images obtained with cantilevers having different properties [2], and to measure force fields above a solid surface with atomic precision [3].

There are numerous methods of calibrating the stiffness of AFM cantilevers [4, 5] which can mainly be divided into *dimensional methods* based on the calculation of the stiffness from dimensions and material properties [6], *dynamic methods* based on measuring resonance properties [7–9] and *static methods* where the cantilever bending is measured as a function of the applied force [10–13]. All of these methods have certain requirements and limitations that are often not compatible with the needs of a non-destructive determination of the stiffness in a given AFM setup. The thermal method [7] requires a spectrum analyser to record the thermally excited cantilever motion and correction factors for the energy distribution over the fundamental resonance and higher harmonics [14, 15]. Another method introduced by Sader *et al* [8] can easily be applied in fluids of known density and viscosity like air but is not applicable in the UHV. Methods adding particles of known mass to the cantilever [9] or measuring the deflection while the cantilever is pushed onto a calibrated reference cantilever [10] are destructive or possibly contaminating and time consuming.
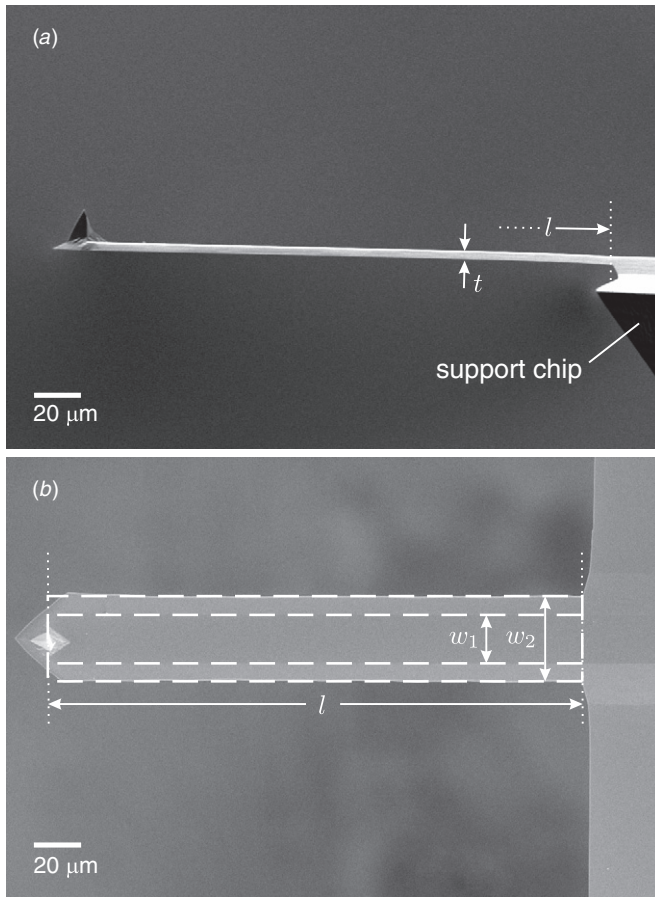
Figure 1. SEM micrographs of cantilever D 5 taken to obtain its precise dimensions. (*a*) Side view revealing the thickness *t*. (*b*) Top view revealing the cantilever length *l* as well as the width w_1 of the tip side and the width w_2 of the back side of the cantilever.

Here, we describe a method combining an analysis of cantilever dimensions, often provided by the manufacturer, with a dynamic analysis that can easily be performed in most ultra-high vacuum compatible NC-AFM systems. Our method is based on the method introduced by Cleveland *et al* [9] but we apply a tip mass correction derived from the ratio of the eigenfrequencies of the fundamental and first harmonic mode of the cantilever oscillation [16]. We demonstrate the importance of the tip mass correction and verify stiffness values by a comparison to results from a high-precision static method determining a force–bending curve. We aim for high precision in determining the stiffness and perform a rigorous analysis of measurement uncertainty. While eliminating systematic errors, we determine the error of measured quantities by a statistical analysis and determine the error of the calculated final values by considering error propagation [17].

2. Stiffness determined from cantilever dimensions

The stiffness of a cantilever as shown in figure 1 can be calculated from its dimensions as

$$k_{\text{dim}} = \frac{3EI}{l^3} \tag{1}$$

with *E* as Young's modulus, *I* as the moment of inertia of the cantilever beam and *l* as the length of the cantilever [6]. The moment of inertia of a rectangular cantilever is given by

$$I_{\text{rectangular}} = \frac{1}{12} w t^3 \tag{2}$$

with width *w* and thickness *t* [6]. Most commercially available single-beam cantilevers, however, have a trapezoidal cross-section where w_1 and w_2 are the width of the tip side and the back side of the cantilever, respectively, as illustrated in the scanning electron microscopy (SEM) micrograph of figure 1(*b*). It is useful to define a mean cantilever width as

$$\overline{w} = (w_1 + w_2)/2 \tag{3}$$

allowing the use of equation (2) also for cantilevers with trapezoidal cross-sections. This approximation yields a slight overestimation of k_{dim} of the order of 2% as derived in appendix A.

We investigate ten silicon cantilevers (Nanoworld AG, Neuchâtel, Switzerland) having resonance frequencies in the range of 50–70 kHz (type FM). The cantilever dimensions for each cantilever are given in table 1 together with other cantilever properties.

These dimensions have been determined by the manufacturer using an optical microscope for determining the length *l* and width *w* and a laser interferometer for determining the thickness *t*. The cantilever length is measured from the attachment point at the support chip to the AFM tip (see figure 1) as this is the point where forces act on the cantilever. For a cross-check of the data provided by the manufacturer in the datasheet, we inspect selected cantilevers by SEM and deduce dimensions from an analysis of micrographs as shown in figure 1. The dimensions of cantilever D 5 as determined by the SEM analysis are, for instance, $l = 227 \pm 12$ μm, $w_1 = 20.8 \pm 1.1$ μm, $w_2 = 35.8 \pm 1.8$ μm and $t = 2.7 \pm 0.2$ μm. As for all other inspected cantilevers, they are in good agreement with the values $l = 229$ μm, $\overline{w} = 30$ μm and $t = 2.9$ μm given in the data sheet. Principally, the SEM should allow the determination of dimensions with higher precision than the optical microscope. Practically, such measurements are, however, hampered by difficulties in the proper alignment, and specifically the precision of thickness measurements by SEM analysis is limited by sample tilting. The strength of the manufacturer's dimensional analysis is the intrinsic precision of the interferometric method for thickness determination and the inspection of the cantilever still being bonded to the wafer from which it is produced. The wafer provides a large plane greatly facilitating perfect alignment so that even optical microscopy yields lateral dimensions with a precision that can hardly be exceeded by SEM analysis without excessive effort in alignment.
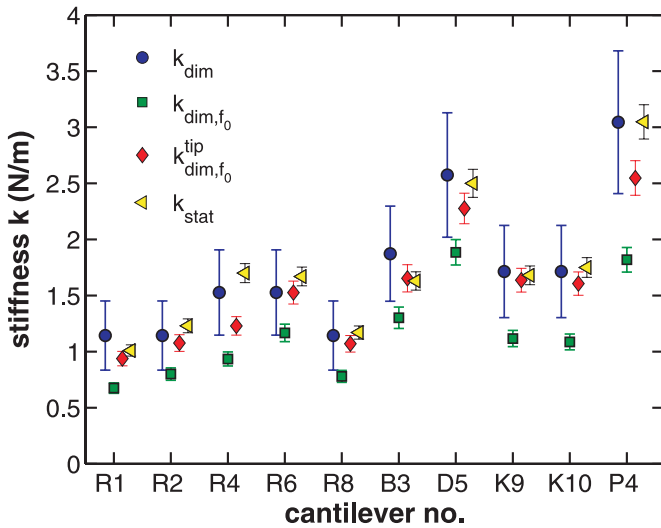
In table 2, we compile stiffness values k_{dim} calculated according to equations (1) and (2) assuming cantilevers with a rectangular cross-section $\overline{w} \times t$. As a material parameter, we use Young's modulus of $E_{\text{Si}(110)} = 169$ GPa [19]. Results are put into graphs in figure 2 (circles) together with the results from other methods where values of k_{dim} are plotted as solid circles. The large error bars (typical uncertainty $\pm 25\%$) mainly stem from the dependence $k \propto t^3$ in combination with the large uncertainty in the thickness measurement typically amounting to $\pm 8\%$.

Table 1. Dimensions of the investigated cantilevers, namely length l, mean width $\overline{w}$ and thickness t as given by the manufacturer (uncertainty $\Delta l = \pm 2.5 \ \mu$m, $\Delta w = \pm 1.5 \ \mu$m and $\Delta t = \pm 0.2 \ \mu$m). Eigenfrequencies f_0 and f_1 (uncertainty $\Delta f_0 = \pm 0.1$ Hz and $\Delta f_1 = \pm 0.5$ Hz) as measured in vacuum [18]. The ratio $\mu = m_{\text{tip}}/m_{\text{beam}}$ and the eigenvalue α_0 are calculated from the ratio f_1/f_0 using equations (5) and (8), respectively (calculated uncertainty $\Delta\mu = 10$ ppm and $\Delta\alpha_0 = 10$ ppm).

Cantilever	l (μm)	$\overline{w}$ (μm)	t (μm)	f_0 (Hz)	f_1 (Hz)	μ	α_0
R 1	224.0	25.0	2.3	52 720.2	336 368.8	0.060 95	1.775 05
R 2	224.0	25.0	2.3	55 792.3	354 867.2	0.054 50	1.784 46
R 4	224.0	26.0	2.5	57 996.8	368 110.7	0.049 85	1.791 39
R 6	224.0	26.0	2.5	62 453.2	396 198.4	0.048 72	1.793 11
R 8	224.0	25.0	2.3	55 308.5	352 451.6	0.058 45	1.778 66
B 3	225.0	23.0	2.8	67 170.6	425 114.0	0.043 06	1.801 77
D 5	229.0	30.0	2.9	68 345.1	430 978.6	0.033 29	1.817 21
K 9	227.0	27.0	2.6	59 968.6	384 813.5	0.072 01	1.759 45
K 10	227.0	27.0	2.6	59 429.1	381 758.0	0.073 97	1.756 75
P 4	224.0	30.0	3.0	69 040.0	440 845.0	0.062 55	1.772 75

Table 2. Cantilever stiffness k_{dim} obtained from a dimensional analysis compared to values k_{dim,f_0} obtained from length, width and resonance frequency of the cantilever and $k_{\text{dim},f_0}^{\text{tip}}$ including a correction for the tip mass. Reference values k_{stat} are obtained from the precision measurement of force–bending curves.
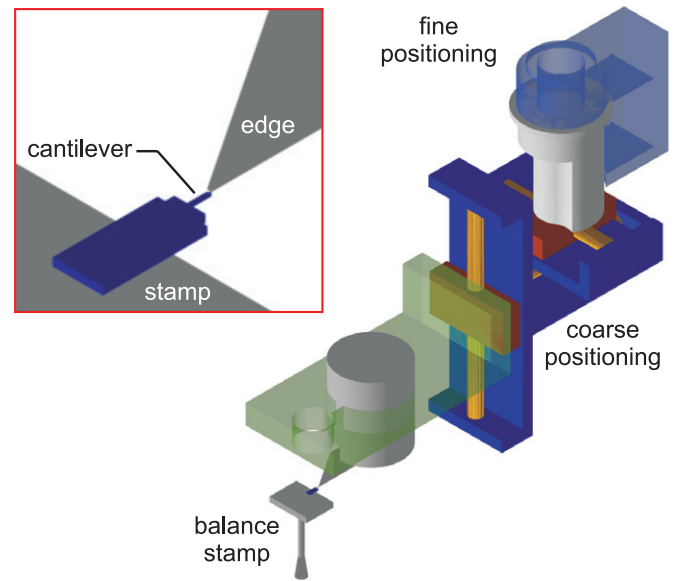
Cantilever	k_{dim} (N m^{-1})	k_{dim,f_0} (N m^{-1})	$k_{\text{dim},f_0}^{\text{tip}}$ (N m^{-1})	k_{stat} (N m^{-1})
R 1	1.1 ± 0.4	0.67 ± 0.07	0.93 ± 0.09	1.01 ± 0.06
R 2	1.1 ± 0.4	0.79 ± 0.08	1.07 ± 0.10	1.23 ± 0.06
R 4	1.5 ± 0.5	0.93 ± 0.09	1.22 ± 0.12	1.70 ± 0.09
R 6	1.5 ± 0.5	1.16 ± 0.11	1.51 ± 0.14	1.67 ± 0.08
R 8	1.1 ± 0.4	0.77 ± 0.08	1.06 ± 0.10	1.17 ± 0.06
B 3	1.9 ± 0.6	1.29 ± 0.13	1.64 ± 0.17	1.63 ± 0.08
D 5	2.6 ± 0.8	1.87 ± 0.16	2.25 ± 0.19	2.50 ± 0.13
K 9	1.7 ± 0.6	1.11 ± 0.10	1.62 ± 0.15	1.68 ± 0.09
K 10	1.7 ± 0.6	1.08 ± 0.10	1.59 ± 0.15	1.75 ± 0.09
P 4	3.0 ± 0.9	1.80 ± 0.16	2.52 ± 0.22	3.05 ± 0.16

Figure 3. Schematic representation of the setup for the static stiffness measurement. The expanded view in the upper left shows the region of the contact between the edge and the tip. The support chip of the cantilever is mounted on the stamp of the balance with the tip pointing upwards.

Figure 2. Comparison of cantilever stiffness determined by different methods. The error bars for k_{dim,f_0} do not include the systematic error introduced by neglecting the tip mass.

3. Stiffness determined from force–bending curves

To verify the results from the dimensional analysis, all cantilevers are investigated in a precision nano-force

measurement setup based on a static measurement of the cantilever bending as a function of the applied force as determined by a balance. This method allows a direct determination of the stiffness k_{stat} from the force–bending curve; however, as it involves pressing the tip against an edge, the method is tip destructive.

The respective setup was originally developed for the calibration of reference cantilevers and micro-manipulation equipment [11] and is schematically depicted in figure 3. The cantilever is mounted with its tip side up on the stamp of an ultra-precision balance having a force resolution of 2 nN (type SC2, Sartorius AG, Göttingen, Germany). A force F is applied to the tip by an edge mounted on a positioning unit allowing for coarse positioning in three dimensions and fine positioning in the vertical direction. For taking a force–bending curve, the fine-positioning device (PIFOC P 721 with digital controller E 750, Physik Instrumente (PI) GmbH & Co. KG, Karlsruhe, Germany) moves the edge along the z coordinate (vertical) in
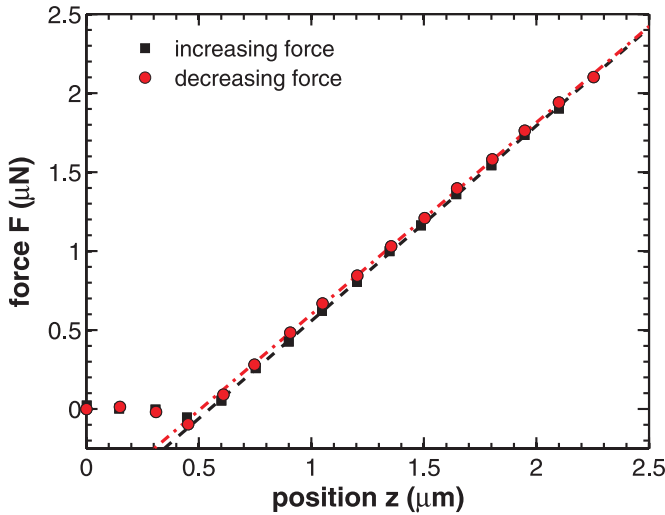
Figure 4. Force–bending curve measured for cantilever R 1 with the static reference method.

contact with the tip over a range of typically 2.5 μm with a positioning accuracy of 1 nm. The maximum force exerted on the tip is typically 4 μN to ensure the validity of Hooke's law over the entire range of bending. By ramping the edge position stepwise up and down in an automated process, a force–bending curve as shown in figure 4 is obtained. This curve exhibits a region of approach ($F = 0$), the snap-to-contact and a region with a linear dependence of the force as a function of the z position. The stiffness of the cantilever is determined from the fit of a straight line to the force–bending curve in its linear region:

$$k_{\text{stat}} = \frac{\Delta F}{\Delta z}. \tag{4}$$

The measurement is repeated 100 times. The average slope is calculated separately for ramping up and down where the hysteresis does not yield results deviating more than 1% from each other. The standard deviation of such a series of measurements is smaller than ± 0.01 N m^{-1} for all cantilevers investigated here. The high reproducibility is obtained by placing the measurement setup in a well-controlled environment of stabilized ambient pressure, temperature and humidity as described in appendix B. Considering the accuracy of the force measurement and systematic errors, e.g. resulting from indenting the tip, the uncertainty limit of the static reference measurement is determined to be below 5% in a conservative estimate.

The stiffness k_{stat} is determined for all cantilevers investigated by the dimensional method and results are compiled in table 2 and shown in figure 2 (triangles). As a notable result, we mention that the deviation of k_{dim} from k_{stat} is generally small (maximum 15%) despite the large uncertainty of k_{dim}. This points to the principal capability of the dimensional method to yield accurate stiffness data.

4. Stiffness determined from dimensions and eigenfrequencies

As an alternative method to determine the stiffness avoiding the shortcomings of the simple dimensional method, it has
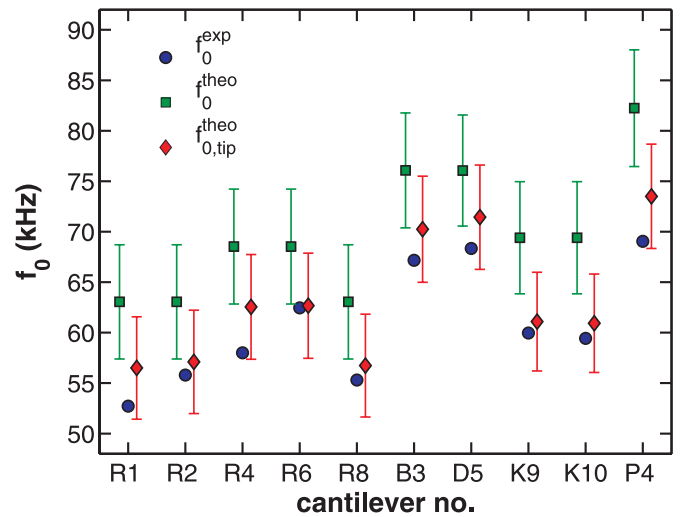
Figure 5. Measured eigenfrequencies f_0^{exp} compared to calculated eigenfrequencies f_0^{theo} based on equation (5) and eigenfrequencies $f_{0,\text{tip}}^{\text{theo}}$ based on equation (5) including tip mass corrected values α_0 determined individually for each cantilever.

been suggested [9] to combine cantilever dimensions with the cantilever eigenfrequency. The eigenfrequency f_n of the nth mode of a rectangular cantilever is given by [20, 6]

$$f_n = \frac{\omega_n}{2\pi} = \frac{\alpha_n^2 t}{2\pi l^2} \sqrt{\frac{E}{12\rho}}, \qquad n = 0, 1, 2, \ldots, \tag{5}$$

with ρ as the density of the cantilever material and α_n as eigenvalues of the Euler–Bernoulli partial differential equation [21] solved to describe the cantilever oscillation[3]. Combining equations (1), (2) and (5) allows one to determine the stiffness while eliminating the critical thickness measurement [4]:

$$k_{\text{dim},f_n} = \frac{2\pi^3 w l^3 f_n^3}{\alpha_n^6} \sqrt{\frac{12^3 \rho^3}{E}}. \tag{6}$$

In the following, this method is used under the assumption that the investigated cantilever has a rectangular cross-section of $\overline{w} \times t$. The more rigorous analysis assuming a trapezoidal cross-section introduced in appendix A yields a difference between the calculations for the rectangular and trapezoidal cross-sections of about 1%. To obtain the eigenvalues α_n, the following equation [14] is solved numerically:

$$\cos \alpha_n \cosh \alpha_n + 1 = 0. \tag{7}$$

For the fundamental mode, the solution is $\alpha_0 = 1.8751$. In figure 5, we compare the eigenfrequencies f_0^{theo} of the investigated cantilevers (squares) calculated according to equation (5) with $\alpha_0 = 1.8751$ and a density of $\rho_{\text{Si}} = 2331$ kg m^{-3} [23] with measured values f_0^{exp} (circles) that can be determined with a precision of ± 0.1 Hz [18]. While the calculated uncertainty in the eigenfrequency is about $\pm 8\%$, we find calculated frequencies typically 15% higher than measured ones. This systematic error stems from neglecting the tip mass that is a significant contribution to the oscillating

---

[3] To be consistent with [6] and our former work [18, 22], we denote the fundamental resonance frequency as f_0 and, therefore, label the solutions α_n of equation (7) as $n = 0, 1, 2, \ldots$, while other authors [14, 16, 20] associate the fundamental mode with $n = 1$.
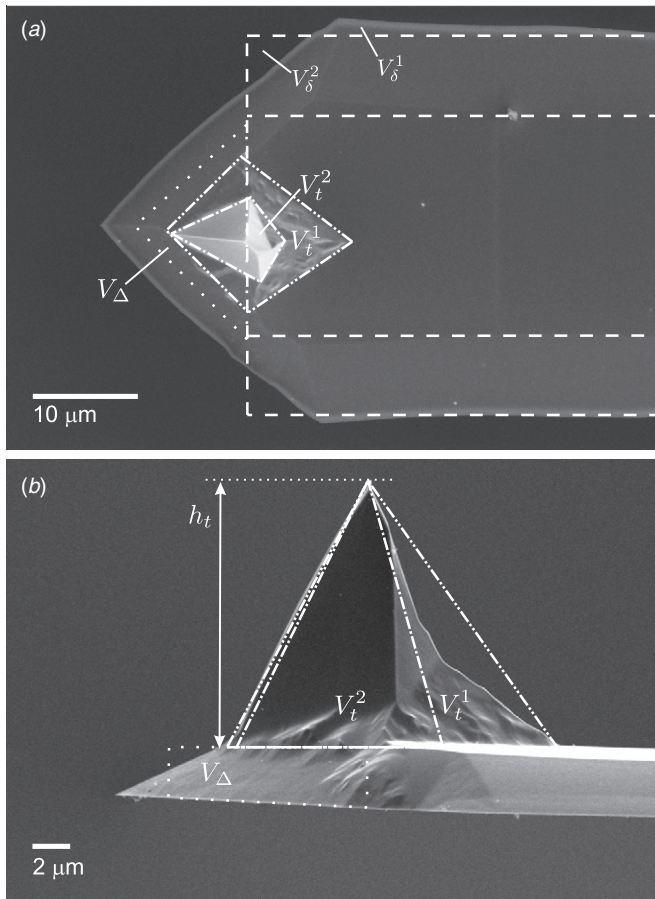
Figure 6. SEM micrographs of details in the tip region of cantilever D 5. (*a*) Top view; (*b*) side view. The meaning of the height and volume quantities shown is explained in the text.

mass for cantilevers and tips of dimensions as investigated here. The error in the calculated eigenfrequency propagates to the stiffness calculation k_{dim,f_0} as is evident from table 2 and figure 2 where the squares are systematically outside the error bars below the stiffness values of the other methods.

To correct for the mass of the tip, we apply an extended cantilever oscillation model [20, 21] and substitute equation (7) by

$$\cos \alpha_n + 1/\cosh \alpha_n + \mu \alpha_n (\tanh \alpha_n \cos \alpha_n - \sin \alpha_n) = 0, \quad (8)$$

where

$$\mu = m_{\mathrm{tip}}/m_{\mathrm{beam}} = m_{\mathrm{tip}}/(\rho w t l) \quad (9)$$

is the ratio between the tip mass m_{tip} and the mass of the cantilever beam. To obtain an estimate for the tip mass, we again employ SEM and try to determine the tip volume from an analysis of SEM micrographs exhibiting details of the tip in the side and top views as shown in figure 6 for the example of cantilever D 5. As the tip has not an ideal pyramidal shape but a more irregularly shaped base, we determine upper and lower limits of the tip volume denoted as V_t^1 and V_t^2 using the rhombic base areas marked in figure 6(*a*) and the tip height h_t obtained from figure 6(*b*).

Apart from the mass of the AFM tip itself, other volume parts at the cantilever end differing from the idealized cantilever (dashed lines in figure 6(*a*)) contribute to the mass correction. In the following, we subsume all of these contributions as the tip mass:

$$m_{\mathrm{tip}} = \rho \left(\frac{V_t^1 + V_t^2}{2} + V_D + V_\delta^1 - V_\delta^2 \right). \quad (10)$$

A significant contribution is the volume V_Δ of the triangular part of the cantilever beyond the tip position. Furthermore, we consider the additional mass caused by the widening of the cantilever (V_δ^1) shortly before its end and the reduction (V_δ^2) due to the triangular shape of the end section, which often cancel each other. Using equations (9) and (10), we obtain $\mu = 0.035 \pm 0.009$ as a mean value defined by the upper and lower limits $V_t^1 + V_\Delta$ and $V_t^2 + V_\Delta$. Solving equation (8) for this tip mass ratio yields $\alpha_0 = 1.815 \pm 0.015$ for cantilever D 5, which is a deviation of 3.2% from the value of $\alpha_0 = 1.8751$ determined for a cantilever without a tip.

Seeking a procedure yielding μ without the time-consuming analysis of SEM micrographs, we follow a procedure introduced by Allen *et al* who demonstrated that μ can be determined from the ratio f_1/f_0 between the first and second eigenfrequencies of the cantilever [16] by using the relation

$$f_1/f_0 = \alpha_1^2/\alpha_0^2 \quad (11)$$

that is evident from equation (5). To accomplish this, a system of equation (11) and equation (8) for $n = 0$ and $n = 1$ is solved to determine the three unknowns μ, α_0 and α_1 with a more detailed description given in appendix C. For cantilever D 5, we obtain $\mu = 0.033\,29 \pm 0.000\,01$ and $\alpha_0 = 1.817\,21 \pm 0.000\,01$, which is well in agreement with the value determined from the SEM analysis. The high accuracy in the measurement of the eigenfrequencies yields an extremely low uncertainty of the calculated mass ratio μ and the eigenvalue α_0. In table 1, the values of μ and α_0 obtained from the ratio f_1/f_0 are given for all investigated cantilevers. The tip mass ratios differ by a factor of more than 2 from each other, motivating an individual measurement for each cantilever instead of using a standard value for all cantilevers. Such calculations are performed within minutes with the help of the algorithm provided in the supplementary materials available at stacks.iop.org/MST/23/045401. To illustrate the effect of the tip mass correction on results from equation (5), we determine eigenfrequencies $f_{0,\mathrm{tip}}^{\mathrm{theo}}$ with tip mass correction and include them in figure 5 (diamonds). They agree well with experimental values (circles).

The spring constants $k_{\mathrm{dim},f_0}^{\mathrm{tip}}$ calculated using equation (6) with tip mass corrections according to equations (8) and (9) are included in table 2 and shown in figure 2 (diamonds) for comparison. Their uncertainty is $\pm 7\%$ and we generally find a rather perfect agreement of these values with k_{stat} values (triangles). Although this method does not require a measurement of the cantilever thickness, a nonuniform thickness along the cantilever beam can significantly change its dynamic behaviour [16], which may be the reason for the results of cantilever R 4 being less consistent than the others. The dimensions of cantilevers R 4 and R 6 as well as the calculated values of μ are almost identical; however, their measured eigenfrequencies differ significantly. As also k_{stat} values for R 4 and R 6 are almost identical, it is clear that

the difference in $k_{\mathrm{dim},\mathrm{f}_0}$ is an artefact and points to a limitation of the precision of $k_{\mathrm{dim},\mathrm{f}_0}^{\mathrm{tip}}$ under certain circumstances. The average deviation between $k_{\mathrm{dim},\mathrm{f}_0}^{\mathrm{tip}}$ and k_{stat} is 9% if we do not consider the outlier result of cantilever R 4. This is a dramatic improvement in uncertainty compared to the values $k_{\mathrm{dim},\mathrm{f}_0}$.

5. Discussion

We introduce a non-destructive method for the precise determination of the stiffness of silicon cantilever beams with a trapezoidal cross-section that solely requires a dimensional analysis of the cantilever and the measurement of eigenfrequencies. The obtained precision of typically 7% is close to what is possible at best according to the available literature [12, 13] and our own experience. Even with a most sophisticated setup and great effort in optimization as demonstrated for the static method to determine k, an uncertainty of ± 5% is the best to be claimed. The dimensional/dynamic method introduced here is best suited for the *in situ* characterization of cantilevers for ultra-high vacuum NC-AFM as such systems allow for a precise determination of eigenfrequencies. A limitation may, however, be the detection bandwidth of the NC-AFM system that needs to be 2 MHz, for instance, for 300 kHz cantilevers frequently used in NC-AFM measurements. If reliable plan view dimensions are available from the cantilever manufacturer, the entire characterization can be accomplished within 15 min when using automated control and data analysis software to measure f_0 and f_1, calculate α_0 and finally calculate $k_{\mathrm{dim},\mathrm{f}_0}$ according to equation (6).

The uncertainty in the material constants used is not a limitation for the precision of stiffness determination when cantilevers made of monocrystalline silicon are used. Accurate values for ρ and E are available in the literature [19, 23–25] and their variation with temperature and the degree of doping is small. The temperature dependence of Young's modulus is approximately -60 ppm K^{-1} in the room temperature region, which can be neglected in our uncertainty considerations [25]. The cantilevers investigated here are made of n$^+$ silicon having a specific resistance of 0.01–0.02 Ω cm. A typical doping is about 10^{19} P-atoms cm^{-3}. The corresponding Young's modulus has been found to be $E_{110}^{\mathrm{doped}} = 167.4$ GPa instead of $E_{110} = 169.0$ GPa for undoped silicon [24]. The decrease of E by 1% would yield k_{dim} values decreased by -1% and $k_{\mathrm{dim},\mathrm{f}_0}$ values increased by $+1.3$%. This demonstrates that also the influence of doping on the stiffness determination is small.

A limitation of the method are systematic errors introduced by faults and inhomogeneities in the cantilever thickness caused by disturbances during etching [16], and such errors are hard to quantify. Dimensional inhomogeneity is most probably the cause of the inconsistency found for cantilever R 4. Having examined some ten cantilevers, we find that there are one or two specimens where such problems arise.

While we demonstrate the method for monocrystalline silicon cantilevers commonly used in ultra-high vacuum NC-AFM, it can in principle be used also for cantilevers with a different shape and cantilevers made from different materials. The feasibility of our approach critically depends on the availability of valid physical models for the description of the oscillation of a cantilever with a specific geometry and precise values for the material constants of the respective material it is made of. We anticipate that our approach is least applicable to cantilevers with a coating as the determination of precise parameters for modelling the coating is most difficult in practice. A surprising result of our study is, however, that the very simple approach of calculating the stiffness solely from the cantilever dimensions according to equations (1), (2) and (3) is a good alternative in cases where utmost precision is not needed. This procedure yields a considerably larger uncertainty; however, in our measurements, the deviation from the reference values never exceeds 15%.

Appendix A. Corrections for cantilevers with a trapezoidal cross-section

The moment of inertia of a cantilever having a trapezoidal cross-section is given by [26]

$$I_{\mathrm{trapezoidal}} = \frac{t^3\left(w_1^2 + 4w_1 w_2 + w_2^2\right)}{36(w_1 + w_2)}. \qquad (A.1)$$

Inserting equation (A.1) into equation (1) yields $k_{\mathrm{dim}}^{\mathrm{trap}}$ while the approach presented in section 2 yields $k_{\mathrm{dim}}^{\mathrm{rect}}$ from inserting equation (2) into equation (1). The deviation between results calculated according to the two approaches is

$$\frac{k_{\mathrm{dim}}^{\mathrm{rect}}}{k_{\mathrm{dim}}^{\mathrm{trap}}} = \frac{6\overline{w}^2}{w_1^2 + 4w_1 w_2 + w_2^2} = 1.02 \qquad (A.2)$$

using the dimensions of cantilever D 5 obtained by SEM ($l = 227$ μm, $w_1 = 20.8$ μm, $w_2 = 35.8$ μm, $t = 2.7$ μm and $\overline{w} = 28.3$ μm). This indicates that the usage of the mean width yields a slight overestimation of the cantilever stiffness of typically 2%, which is small compared to the general uncertainty of this method.

The method presented in section 4 can also be modified for cantilevers with trapezoidal cross-sections

$$k_{\mathrm{dim},f_n}^{\mathrm{trap}} = \frac{36\sqrt{2}f_n^3\pi^3 l^3(w_1 + w_2)^2}{\alpha_n^6\sqrt{w_1^2 + 4w_1 w_2 + w_2^2}}\sqrt{\frac{\rho^3}{E}} \qquad (A.3)$$

having equation (5) combined with equations (1) and (A.1) instead of equation (2).

When comparing the exact expression for the trapezoidal cantilever to the simplified expression for the rectangular cantilevers, we obtain in this case

$$\frac{k_{\mathrm{dim},f_n}^{\mathrm{rect}}}{k_{\mathrm{dim},f_n}^{\mathrm{trap}}} = \sqrt{\frac{3}{18}}\frac{\sqrt{w_1^2 + 4w_1 w_2 + w_2^2}}{\overline{w}} = 0.988 \qquad (A.4)$$
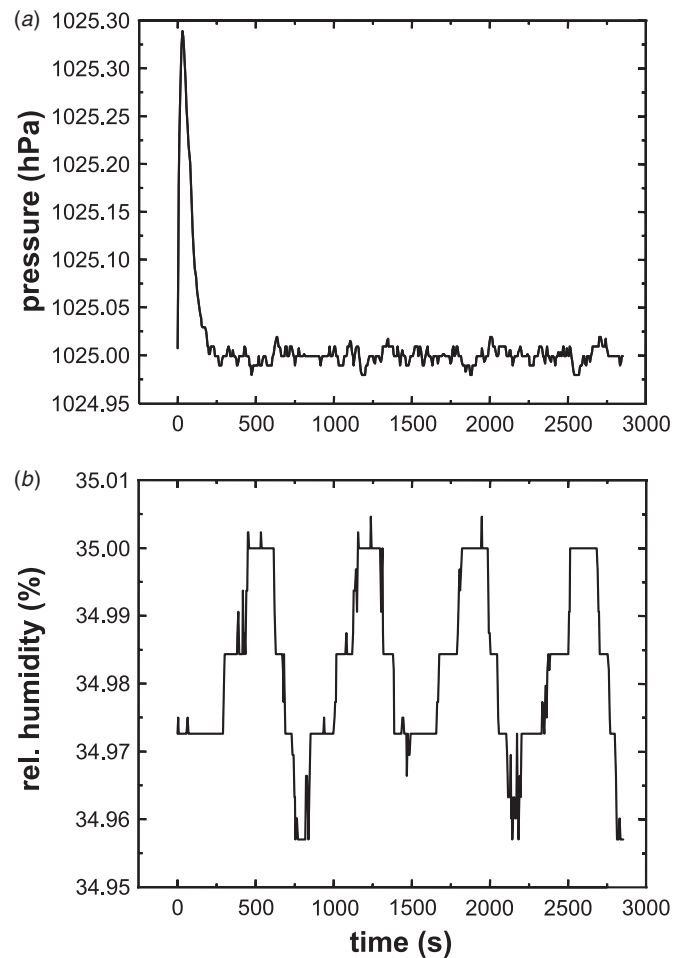
Figure B1. View on the environmentally controlled chamber housing the stiffness measurement system with removed front cover. The main components are (1) coarse and fine positioning units, (2) interaction zone with edge acting on the tip of the cantilever mounted on a balance stamp, (3) ultra-precision scale, (4) pressure gauge with control unit and (5) water container for temperature stabilization.

using the dimensions of cantilever D 5. This results in a slight underestimate (1.2%) of the stiffness of trapezoidal cantilevers when the approximation for rectangular cantilevers is used.

Appendix B. Environmental stabilization of the static stiffness measurement setup

To reproducibly provide identical environmental conditions for measurements of k_{stat}, the setup for the static stiffness measurement is placed in a sealed chamber shown in the photograph of figure B1 with the front cover opened. The pressure inside the chamber as well as the humidity is controlled actively by homemade regulation systems (pressure gauge Model 370, Setra Systems Inc., Boxborough, MA, USA; humidity sensor HygroClip-S, ROTRONIC Messgeräte GmbH, Ettlingen, Germany) while the interior temperature is passively stabilized by the large heat capacity of the aluminium case (about 230 kg) and by the presence of 40 L of water. The environmental parameters are set to values of typically 1030 hPa for the pressure and 40.00% for the humidity while the temperature is room temperature that is externally stabilized to 22 °C. This allows for a stabilization of the pressure with a precision of ± 1 Pa and the relative humidity to be stabilized within $\pm 0.02\%$ rH as demonstrated in figure B2 while the typical drift of temperature is smaller than 10 mK h^{-1}. To achieve these conditions, the setup has to be equilibrated for about 5 h before a series of measurements is taken that typically takes 15 h for one cantilever. While the stabilization of temperature and humidity mainly reduces the instrumental drift, the stabilization of the ambient pressure reduces the noise in the force measurement from a standard deviation of 25 nN without stabilization to a standard deviation of 5 nN with active stabilization as demonstrated


Figure B2. Temporal development of pressure (*a*) and humidity (*b*) in the environmentally controlled chamber for activated regulation systems. The peak in (*a*) is due to the onset of pressure regulation.
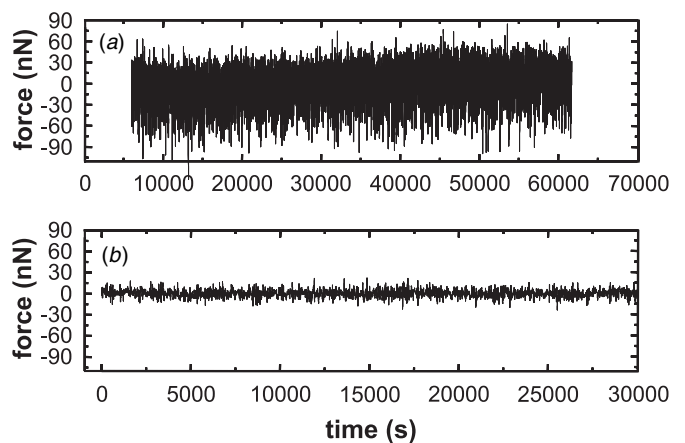
Figure B3. Demonstration of the reduction of the noise floor in the force measurement yielded by the stabilization of the ambient pressure. (*a*) Deviation of force as measured by the precision balance from the mean value without stabilization. (*b*) The same deviation measured with active stabilization.

in figure B3. These measures of stabilization guarantee that stiffness results are not even slightly affected by environmental conditions.

(a)

(b)
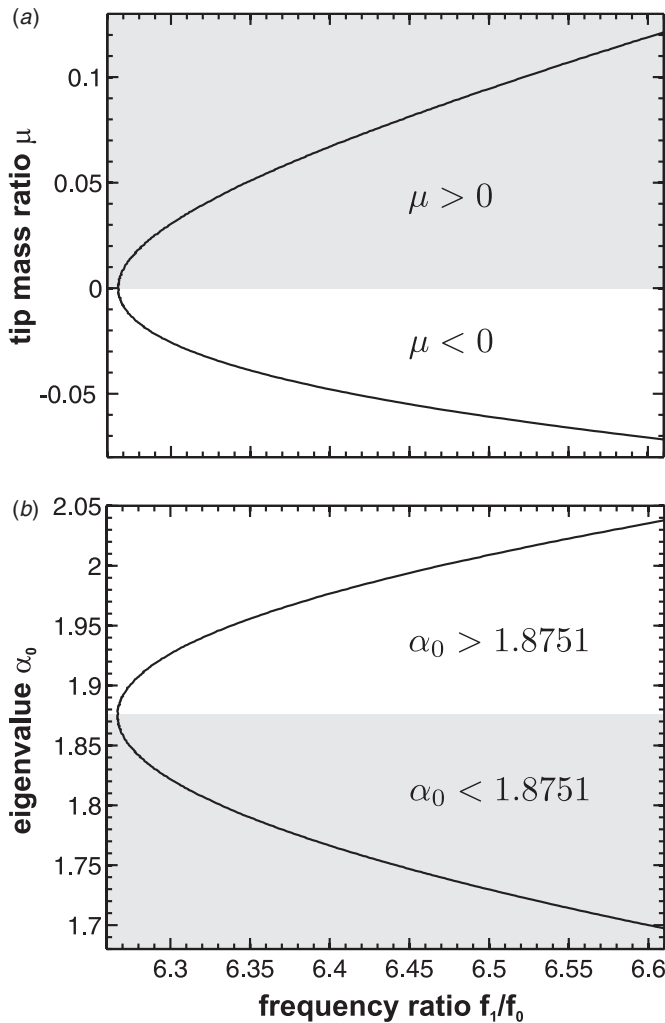
Figure C1. Solutions of equation (8) for a cantilever with a finite tip mass $m_{tip} = \mu \rho w t l$. (*a*) Tip mass ratio μ as a function of the frequency ratio f_1/f_0. (*b*) Eigenvalue α_0 as a function of the frequency ratio f_1/f_0. Shaded areas denote the regions for a positive tip mass correction.

Appendix C. Detailed discussion of tip mass correction

Equation (8) does not allow a straightforward calculation of the tip mass ratio μ as it contains the eigenvalue α_n as a second unknown variable. However, by establishing a relation between the eigenfrequencies f_0, f_1 and the eigenvalues α_0, α_1 for the fundamental and the first harmonic mode of the cantilever via equation (11), μ and α_0 can be determined as a function of the ratio of eigenfrequencies f_1/f_0. The respective results are shown in figure C1. Although α_1 is not shown here, it can be obtained from the ratio f_1/f_0 and α_0 related by equation (11). The function is valid for positive and negative tip mass corrections yielding positive or negative values for μ. Here, we can restrict the discussion to a positive mass ratio μ located in the upper branch of figure C1(*a*) while the corresponding α_0 is found on the lower branch of figure C1(*b*). Although this is the general case, a positive tip mass is not always obvious. As a special case, for instance, picket-shaped cantilevers can be modelled as rectangular

cantilevers with a negative tip mass [27]. To decide whether the tip mass is positive or negative, we use the following expression, derived from equation (5), to obtain a rough estimate of α_0 from the cantilever dimensions and its fundamental mode eigenfrequency:

$$\alpha_0 = l \sqrt{\frac{2\pi f_0}{t}} \sqrt{\frac{12\rho}{E}}. \qquad (C.1)$$

The uncertainty using this method for the stiffness determination is over 30% because $k_{\mathrm{dim}, f_0} \propto \alpha_0^{-6}$. However, the results of relation C.1 are precise enough to decide whether the tip mass is positive or negative, as for a significant tip mass the position in the upper or lower half of the graph of figure C1(*b*) is obvious. For cantilever D 5, we obtain $\alpha_0 = 1.78 \pm 0.07$ from equation (C.1), which is obviously lower than 1.8751 and, therefore, indicates that the tip mass is positive.

References

[1] Bippes C A and Muller D J 2011 High-resolution atomic force microscopy and spectroscopy of native membrane proteins *Rep. Prog. Phys.* **74** 086601
[2] Giessibl F J 1997 Forces and frequency shifts in atomic-resolution dynamic-force microscopy *Phys. Rev.* B **56** 16010–5
[3] Ashino M, Obergfell D, Haluska M, Yang S H, Khlobystov A N, Roth S and Wiesendanger R 2009 Atomic-resolution three-dimensional force and damping maps of carbon nanotube peapods *Nanotechnology* **20** 264001
[4] Clifford C A and Seah M P 2005 The determination of atomic force microscope cantilever spring constants via dimensional methods for nanomechanical analysis *Nanotechnology* **16** 1666–80
[5] Gibson C T, Smith D A and Roberts C J 2005 Calibration of silicon atomic force microscope cantilevers *Nanotechnology* **16** 234–8
[6] Chen C J 1993 *Introduction to Scanning Tunneling Microscopy* (New York: Oxford University Press)
[7] Hutter J L and Bechhoefer J 1993 Calibration of atomic-force microscope tips *Rev. Sci. Instrum.* **64** 1868–73
[8] Sader J E, Chon J W M and Mulvaney P 1999 Calibration of rectangular atomic force microscope cantilevers *Rev. Sci. Instrum.* **70** 3967–9
[9] Cleveland J P, Manne S, Bocek D and Hansma P K 1993 A nondestructive method for determining the spring constant of cantilevers for scanning force microscopy *Rev. Sci. Instrum.* **64** 403–5
[10] Gibson C T, Watson G S and Myhra S 1996 Determination of the spring constants of probes for force microscopy/spectroscopy *Nanotechnology* **7** 259–62
[11] Peiner E, Doering L, Brand U, Christ A, Isenberg G and Balke M 2006 Force calibration of micro pipettes for single-cell probing *18th IMEKO World Congress (Rio de Janeiro, Brazil, 17–22 September 2006)* pp 100–16
[12] Langlois E D, Shaw G A, Kramar J A, Pratt J R and Hurley D C 2007 Spring constant calibration of atomic force microscopy cantilevers with a piezosensor transfer standard *Rev. Sci. Instrum.* **78** 093705
[13] Clifford C A and Seah M P 2009 Improved methods and uncertainty analysis in the calibration of the spring constant of an atomic force microscope cantilever using static experimental methods *Meas. Sci. Technol.* **20** 125501
[14] Butt H-J and Jaschke M 1995 Calculation of thermal noise in atomic force microscopy *Nanotechnology* **6** 1–7

[15] Cook S, Schäffer T E, Chynoweth K M, Wigton M, Simmonds R W and Lang K M 2006 Practical implementation of dynamic methods for measuring atomic force microscope cantilever spring constants *Nanotechnology* **17** 2135–45

[16] Allen M S, Sumali H and Penegor P C 2009 DMCMN: experimental/analytical evaluation of the effect of tip mass on atomic force microscope cantilever calibration *J. Dyn. Syst. Meas. Control* **131** 064501

[17] Grabe M 2005 *Measurement Uncertainties in Science and Technology* (Berlin: Springer)

[18] Lübbe J, Tröger L, Torbrügge S, Bechstein R, Richter C, Kühnle A and Reichling M 2010 Achieving high effective Q-factors in ultra-high vacuum dynamic force microscopy *Meas. Sci. Technol.* **21** 125501

[19] Wortman J J and Evans R A 1965 Young's modulus, shear modulus, and Poisson's ratio in silicon and germanium *J. Appl. Phys.* **36** 153–6

[20] Elmer F J and Dreier M 1997 Eigenfrequencies of a rectangular atomic force microscope cantilever in a medium *J. Appl. Phys.* **81** 7709–14

[21] Lozano J R, Kiracofe D, Melcher J, Garcia R and Raman A 2010 Calibration of higher eigenmode spring constants of atomic force microscope cantilevers *Nanotechnology* **21** 465502

[22] Lübbe J, Temmen M, Schnieder H and Reichling M 2011 Measurement and modelling of non-contact atomic force microscope cantilever properties from ultra-high vacuum to normal pressure conditions *Meas. Sci. Technol.* **22** 055501

[23] Lide D R and Frederikse H P R 2003 *CRC Handbook of Chemistry and Physics* 83rd edn (Boca Raton, FL: CRC Press)

[24] Hall J J 1967 Electronic effects in the elastic constants of *n*-type silicon *Phys. Rev.* **161** 756–61

[25] Hopcroft M A, Nix W D and Kenny T W 2010 What is the Young's modulus of silicon? *J. Microelectromech. Syst.* **19** 229–38

[26] Poggi M A, McFarland A W, Colton J S and Bottomley L A 2005 A method for calculating the spring constant of atomic force microscopy cantilevers with a nonrectangular cross section *Anal. Chem.* **77** 1192–5

[27] Kiracofe D and Raman A 2010 On eigenmodes, stiffness, and sensitivity of atomic force microscope cantilevers in air versus liquids *J. Appl. Phys.* **107** 033506